Geometrically Structured Microtumors in 3D Hydrogel Matrices

*Thomas G. Molley, Xiaochun Wang, Tzong-tyng Hung, Pavithra B. Jayathilaka, Jia-Lin Yang, and Kristopher A. Kilian**

During cancer progression, a growing tumor encounters variation in the surrounding microenvironment leading to a diverse landscape at the tumor–matrix interface. Topological cues at the interface are believed to influence invasive characteristics; however, most laboratory models involve tumor spheroids that develop a uniform geometry within a homogenous hydrogel. In this communication, a method for templating hydrogels in well-defined 3D architectures is reported. Using melanoma as a model cancer, fabrication of geometrically structured model tumors in a myriad of shapes and sizes is demonstrated. These microtumors can be encapsulated in virtually any polymeric matrix, with demonstrations using poly(ethylene glycol) and gelatin-based hydrogels. Light sheet imaging reveals uniform viability throughout with regions of high curvature at the periphery influencing cellular heterogeneity. These hydrogel encapsulated microtumors can be harvested and implanted in animal models, providing a unique xenograft system where relationships between geometry, progression, and invasion may be systematically studied.

Tumors reside in complex 3D microenvironments with spatiotemporal variations in soluble signals, extracellular matrix components, biomechanical parameters, and are comprised of a heterogeneous populations of multiple cell types. This complexity challenges researchers who aim to deconstruct the microenvironment-function relationships underlying tumor pathology. Most commonly, cancer cells are cultured on 2D plastic dishes given the relative ease of assessing simple measures like proliferation and migration; however, these conditions are not representative of native tissue states and poorly capture crucial properties for accurate disease modeling.[1–3] Tumor spheroids attempt to bridge the gap between planar cultures and true tumor architecture with controlled assembly of 3D cancer cell aggregates; however, spheroid cultures offer limited control over this multivariate parameter space, take time to develop, and can be difficult to fabricate reproducibly.[4–6]

In an effort to deconstruct these complexities in a more systematic way, we previously demonstrated how a microcontact printing based technique on hydrogels can confine cancer cells in 2D microaggregates. While these micropatterned cultures of cells are considerably less complex than a 3D aggregate, they offer greater control over underlying biophysical and biochemical properties, and invasive spreading is readily quantitated. For instance, we showed how perimeter geometry in 2D cancer cell aggregates can spatially organize cell phenotype, where tumorigenic cells preferentially reside on regions of positive curvature at the perimeter.[7,8] While model 2D engineered extracellular matrices provide improved control of microenvironment parameters, it is critical to build platforms engineered in 3D to better recreate physiologically relevant conditions. Recently, developments of 3D microniches for somatic and cancer cells using photolithographic techniques have created high-throughput models of cells with controlled geometry, volume, and shape.[9–13] However, current photolithography approaches are limited to projections of 2D shapes in a third dimension which only allows for curvature along one axis, are limited to small volumes, and have not been extended to in vivo applications.[14] It remains challenging to create reproducible 3D model matrices where the mechanical microenvironment surrounding a population of cells can be controlled with defined architecture.

In this communication, we demonstrate a replica molding approach with 3D printing to pattern tumors with varied topologies on three distinct engineered hydrogel matrices. To accurately assess tumor structure-function relationships, we

T. G. Molley, Prof. K. A. Kilian
School of Materials Science and Engineering
University of New South Wales
Sydney, NSW 2052, Australia
E-mail: k.kilian@unsw.edu.au

Dr. X. Wang, J. L. Yang
Prince of Wales Clinical School
University of New South Wales
Sydney, NSW 2052, Australia

Dr. T. T. Hung
Biological Resources Imaging Laboratory
Mark Wainwright Analytical Centre
University of New South Wales
Sydney, NSW 2052, Australia

P. B. Jayathilaka, Prof. K. A. Kilian
School of Chemistry
Australian Centre for Nanomedicine
University of New South Wales
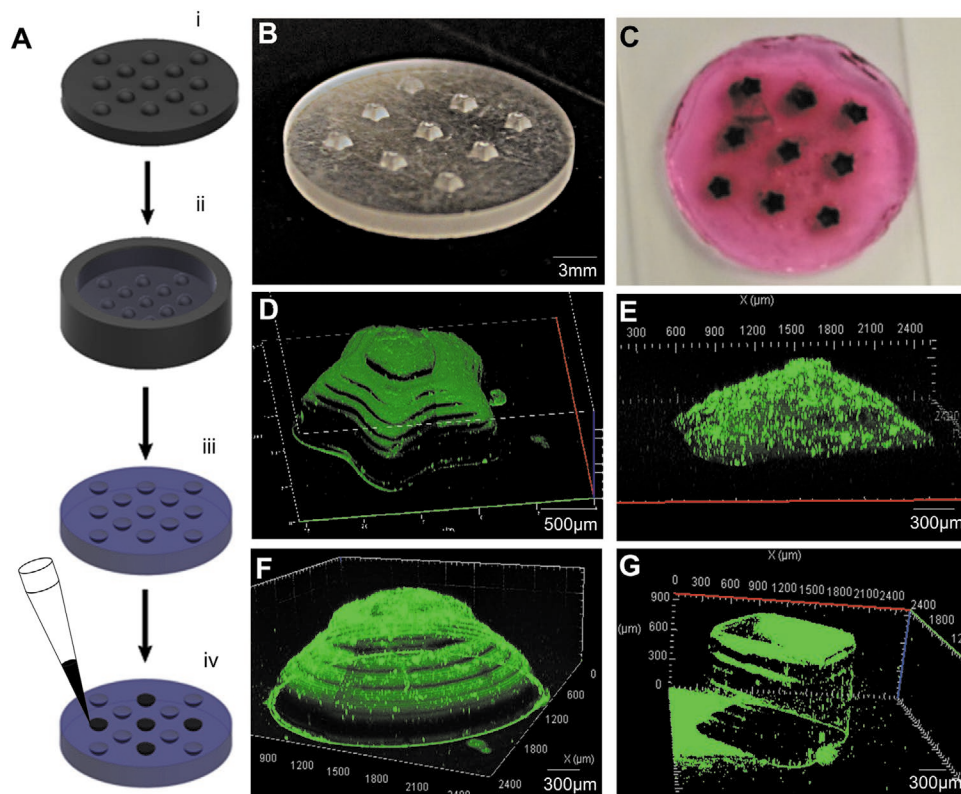Sydney, NSW 2052, Australia

Figure 1. Schematic and characterization of templated hydrogel formation. A-i) A template with the desired inverse topology is 3D printed with resin or plastic, ii) and is placed in a watertight holder. A prehydrogel solution is added on top of the mold and allowed to crosslink following iii) removal of the hydrogel from the template. iv) The template is stored in water until ready to have cells seeded in the cavities. B) A macro image of an SLA printed star shaped template. C) Macro Image of templated PEGDM hydrogel with B16F0 cells loaded at 200 000 000 million cells mL^{-1} after 3 d culture. D–G) Confocal z-stack reconstructions of fluorescent protein (10 µg mL–1 Alexa-488 fibrinogen) adsorbed to the cavity wall surfaces.

developed protocols for tissue clearing and imaging deep into large tumor volumes. We further show the potential for these hydrogel-stabilized geometric structured tumors to be transplanted in vivo as a new class of tumor model where multiple biophysical cues can be defined before implantation.

The design and fabrication process from printing to cell seeding is shown in **Figure 1**A. The first step involves fabricating 3D printing molds with the desired topologies on the template base (Figure 1A-i). Stereolithographic (SLA) 3D printers typically have higher resolution than standard extrusion printers as well as the hydrophobicity of the molds will aid in removing casted hydrogels.[15] Therefore, an SLA printer was chosen to fabricate our molds. By printing a template first with resin, we achieve higher resolution than conventional hydrogel bioprinters with potential for researchers to adopt this approach using any simple 3D printer available in most laboratories. 3D printing the templates also provides the combination of easy access, inexpensive and fast scalability, and parallel throughput. Once the templates were made, a prehydrogel solution was cast onto the template in watertight molds and allowed to crosslink (Figure 1A-ii). Here, any hydrogel may be used with any crosslinking method; however, it should be noted that some gels may not hold their shape when removed from the mold if it is not sufficiently nonwetting or if the polymer rigidity is too low. For this study, end-functionalized poly(ethylene glycol) (PEG) was first used given its wide use in the soft biomaterials

field, ease of crosslinking, and nonwetting behavior that enable easy removal from the mold.[16–19] Once removed, the hydrogel contains a cavity with the inverse topology of the 3D printed molds. Adhesion proteins were physically entrapped at the interface through deposit in the semi-dried microwells (here, 25 µg mL^{-1} fibronectin) and the entire construct was sterilized for 30 min under UV before storage and prior to cell seeding (Figure 1A-iii,iv).

Scanning electron microscopy (SEM) and macro images were collected to characterize the shape and size of the printed molds (Figure 1C and Figure S1G–J, Supporting Information). Initial molds of hemisphere, cube, pyramid, and star shapes were used with the following rationale: the hemisphere provides a constant curvature and resembles the topology of spherical tumor growth; the cube provides sharp contrast between regions of zero curvature against the high curvature found at the corners; the pyramid provides a shallow curvature in one axis, and zero curvature in another; and the star provides regions of positive and negative curvature at the perimeter of the same microtumor. Using a high-resolution printer, multiple sizes of templates can be fabricated to compare the size effect (Figure S1B–F, Supporting Information). SEM characterization also shows template sizes are within 5% of the computer aided design (CAD) model dimensions. Next, to characterize the casted hydrogel cavity surfaces, fluorescent protein (Alexa-488 Fibrinogen, 10 µg mL^{-1} for 30 min at 22 °C) was adsorbed

to the surfaces before being imaged on a confocal microscope (Figure 1D–G). Analysis of z-stacks gives a layer resolution of our printer at 100 um giving feature control down to 50 μm. As such, for shapes of an mm in depth, ten-layer lines can be used. Here, rastering lines can be seen among the shapes due to the limited resolution of the printers. Over the last couple decades, printer resolution has been decreasing steadily and offers this technique potential to have finer control as new developments are made, namely making shapes smoother and smaller.[20]

In previous experiments, we demonstrated control of cellular heterogeneity at the perimeter in 2D melanoma cell aggregates.[8] To investigate whether perimeter geometric structuring in 3D could similarly direct spatial organization of melanoma cells, we selected murine melanoma cells (B16F0 cells, 200 000 000 cells mL^{-1}) to be cultured in star, hemisphere, and cubic templated gels. The black color seen in the photograph of Figure 1C is attributed to melanin within the high-density aggregates, aiding visualization. However, initial imaging using confocal microscopy did not allow discrimination of cells within the 3D construct due to laser light adsorption by the tumor and melanin. Given the tumor size and the desire to contain tumors in their molds during imaging for preservation of edge contact and geometric fidelity postfixation, we selected lightsheet microscopy for imaging. With large tumor constructs, it is vital to obtain a method to properly image through the entire tumor volume, a caveat associated with current spheroid models.[6,21] For this reason, tissue clearing was needed to properly image the entire tumor volume.[22–25] We began with cubic-2 clearing as a starting point due to its ease of synthesis and high success rate in the literature; however, modifications to timing, washing, and handling were made to accommodate the protocol to our microtumors.[26,27] Primary and secondary antibody staining was performed between the lipid extraction step and index refraction matching without the need for embedding the sample. Nevertheless, even after clearing the melanin was still present and prevented imaging deep into the tissue. Hydrogen peroxide has previously been shown to bleach melanin from melanoma tumors and was therefore chosen to supplement our protocol.[28] We made adjustments to keep the temperature low (37 °C) to reduce bubble formation from within that causes the breakdown of the tumor constructs (Figure S2, Supporting Information). It is also important to note that to achieve adequate bleaching at a lower temperature, the bleaching time was increased from 30 min to 24 h.

To test the cell volume filling and clearing protocols, microtumors of B16F0 cells were seeded and cultured for 5 d. To seed at such high densities, 15 million cells were pelleted in a tube and all supernatant removed from the solution. The cell pellet was agitated to break apart and directly pipetted into the cavities. Care must be taken to ensure a high density of cells when seeding to create microtumors with an adequate size and number of viable cells.

After 5 d of culture, the cells were fixed, cleared, and stained for the nuclei and filamentous actin. Representative reconstructions of the nuclei and cytoskeleton of cells within hemisphere, cubic and star tumors are shown in **Figure 2**A–C. Multiple viewpoints were taken to asses and verify the filling of the entire template volume with tumor cells. This technique enables high resolution scanning and reconstruction of the microtumors,

aiding in both verification to volume filing and the potential for visualization of subpopulations within the tumor construct. Importantly, similar stain intensities of the microtumors' exterior and interior show success of the optimized tissue bleaching and clearing procedure. However, it is worth noting that in a fraction of microtumors, the cells near the surface detach from the walls during processing.

To assess the role of topology in control of tumor heterogeneity, we immunostained our cultures with ABCB5, a well-known molecular marker for melanoma tumorigenicity that is involved in drug-efflux.[29] Melanoma microtumors were fabricated in each of the star, cube, and hemisphere shapes and cultured for 5 d, the length of time that we have previously shown leads to enhancement of tumorigenic stem-fraction at the perimeter.[8] Representative images of microtumors demonstrate complete IgG antibody penetration deep into the tumors (Figure 2D–F); z-stack slices across the tumor volume demonstrate consistent marker expression. The intensity of ABCB-5 staining is consistent throughout the tumor with clear 'hotspots' of activity at perimeter regions, suggestive of interfacial control of tumorigenicity in these 3D microtumors. With tumor volumes of 1–2 mm^3, it is likely that oxygen and nutrient delivery will be limited throughout these large aggregates—as periphery cells deplete them before they can diffuse throughout the tumor—thereby forming hypoxic pockets. Interestingly, small interior voids were observed within the microtumors (Figure 2D–F); however, it is unclear whether these voids are hypoxic niches, or if they arise from cell displacement during processing.

To further explore the generality of our approach, we templated and cultured cells within gelatin-methacryloyl (GelMa) hydrogels, a matrix-mimetic material commonly used in tissue engineering, where stiffness and porosity can be readily tuned.[30] **Figure 3**A shows confocal images of square microtumors made with i) 8 wt%, ii) 10 wt%, and iii) 12 wt% GelMa. Here, rheological measures show storage modulus values of 1.3, 5.5, and 16 kPa, respectively (Figure 3B). Since we observed regional variations of ABCB5 in our PEG-encapsulated microtumors, we selected the melanoma stem cell marker CD271 in 10 wt% GelMa hemispheres to quantify spatial intensity and perimeter enhancement. To do this, we compared molecular marker expression in the outer 20% of different height slices within a z-stack and found a 1.3-fold increase in CD271 expression in cells at the margin. Initial probing shows similar expression profiles for tumors encapsulated within GelMa matrices of all three stiffness (Figure S4, Supporting Information), consistent with our previous work in 2D micropatterned cultures where B16 melanoma cells demonstrate insensitivity to substrate stiffness spanning 1–100 kPa. This proof of concept characterization indicates that we have some control over tumor heterogeneity in our 3D microtumors.

Matrix invasion is one of the first steps preceding tumor metastasis, and embedded tumoroids have been shown to invade into the surrounding matrix.[31] Since GelMa is a crosslinked natural biopolymer derived from collagen, we reasoned that cells at the microtumor boundary would be able to digest the matrix and invade. However, cells at the periphery of our microtumors showed limited signs of invasion into the surrounding matrix after 5 d of culture. We speculate this may be
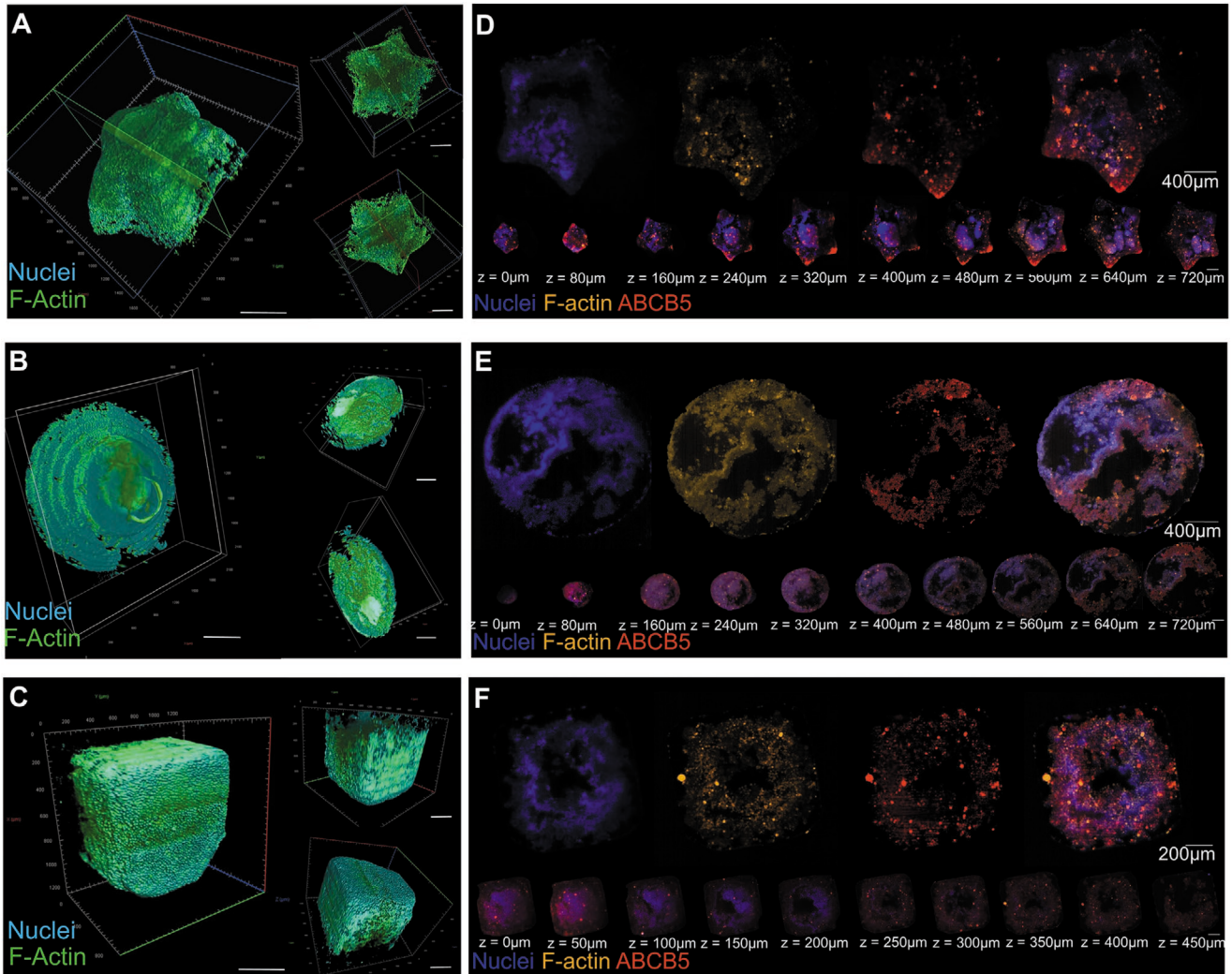
**ADVANCED
SCIENCE NEWS**

www.advancedsciencenews.com

**ADVANCED
BIOSYSTEMS**

www.adv-biosys.com

Figure 2. Visualization of fixed microtumors from lightsheet *z*-stacks. A–C) Representative 3D reconstructions of B16F0 microtumors cultured for 5 d prior to fixation, bleaching, clearing, and staining with Hoechst and Phalloidin for nuclei and F-actin, respectively; scale bars: 400 µm. Lightsheet slices taken from representative *z*-stacks (5x) of D) star, E) hemisphere, and F) cubic tumors stained for nuclei, F-actin, and ABCB-5. Slices for dye breakdowns correspond to 700, 720, and 450 µm for the star, hemisphere, and cubic tumors, respectively; scale bars: D,E) 400 µm, F) 200 µm.

due in part to differences in crosslinking associated with methacrylate polymerization compared to triple helical collagen that is crosslinked by enzymatic means, thereby attenuating degradation by cell-secreted enzymes. As a readily degradable matrix, we templated the melanoma aggregates within a disulfide linked PEG hydrogel with comparable stiffness to our GelMa 12 wt% (Figure 3G,H). Disulfides are readily reduced through numerous mechanisms in biology, and cells have been shown to degrade PEG-based disulfide hydrogels.[32,33] After 7 d of culture, cells clearly degraded and migrated out from the initially defined microtumor architecture, demonstrating complete restructuring of the microenvironment (Figure 3I).

Using both synthetic and natural hydrogel materials, our approach can be used to study in vitro behavior of tumor aggregates. However, there have been limited studies into well-defined tumor aggregates in vivo. Xenograft models typically have cells inoculated in suspension directly to the site of implantation. This invariably leads to limited control over

initial conditions of cell and matrix distribution within the tissue.[34] Considering the tight coordination of cell-matrix interactions that precede invasive phenotypes and signaling, mouse models with precise control of tumor architecture would be advantageous to cancer research. Importantly, our geometric templating approach provides a system where the cells can be preorganized with well-defined topology prior to implantation. This enables investigations of both immortalized cell lines for fundamental knowledge as well as creation of engineered patient tumor grafts for personalized medicine endeavors.

To explore the potential for using our microtumor fabrication approach in vivo, we chose to evaluate subcutaneous xenografts of nondegradable PEG microtumors in C57BL/6 mice since this model is well understood to replicate syngeneic progression.[35] For the implantation, hydrogel matrices surrounding the tumor were cut to contain only one microtumor with ≈200 000 cells (**Figure 4**A). The tumors were implanted subcutaneously into
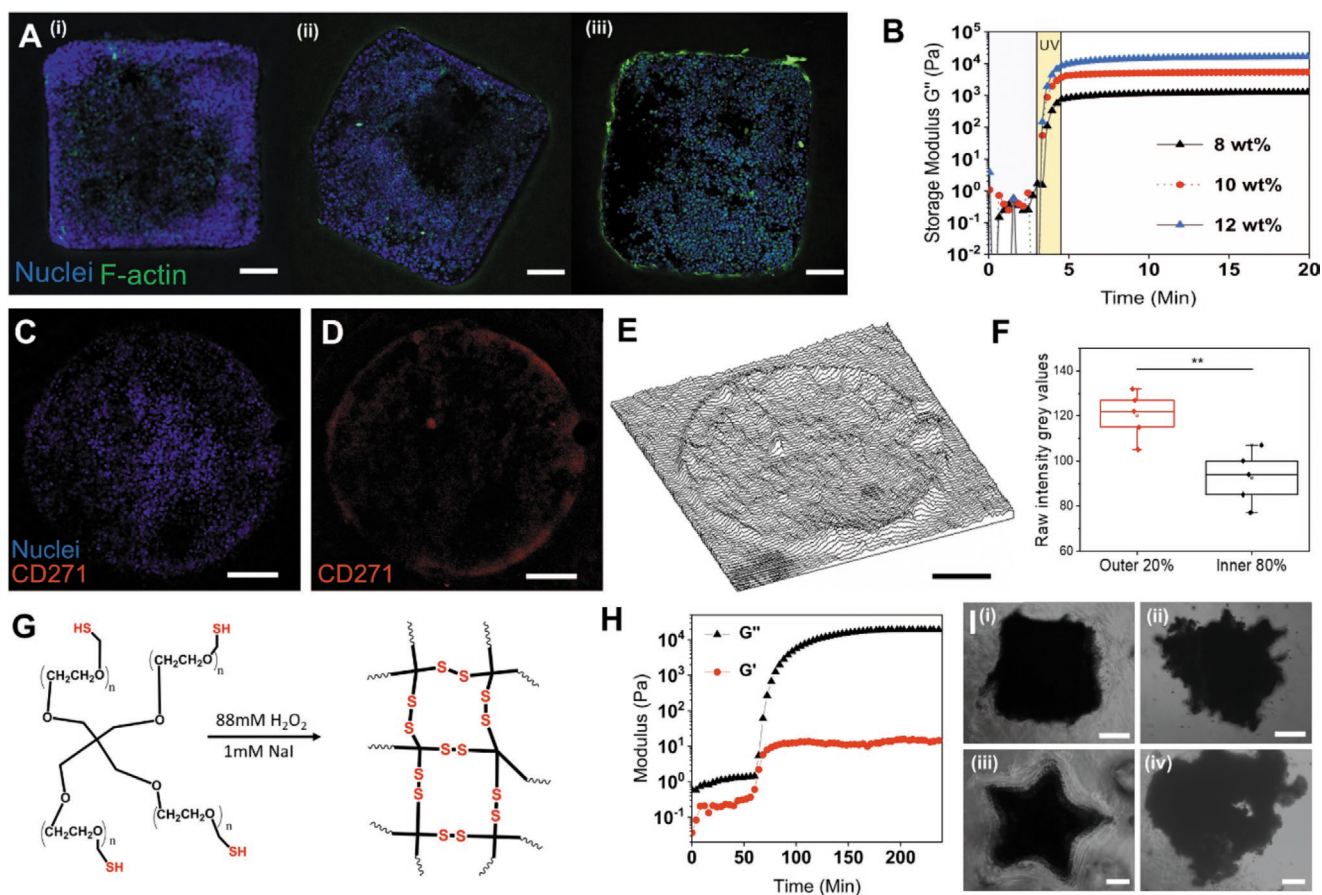
Figure 3. Templating microtumors on GelMa and PEG-SH hydrogels. A) Representative slices of nuclei and actin in i) 8 wt%, ii) 10 wt%, and iii) 12 wt% GelMa after 5 d of culture. B) Rheological measurements on gelation of GelMa after 60 s of UV exposure. C) Composite image of nuclei and CD271 expression in a 10 wt% GelMa hemisphere gel after 5 d. D) The CD271 channel from (C). E) Surface intensity map of CD271 expression from (D) to aid visualization. F) Box plot of average gray intensity values of the outer 20% of hemisphere versus the inner 80% for a 12 wt% GelMa hemisphere z-stack. Slices were taken at different heights in the gel ($N = 5$, $**p < 0.005$, one-way ANOVA test). G) Schematic of four-arm PEG-SH hydrogel. H) Rheological analysis of PEG-SH gelation. I) Optical images of microtumors degrading PEG-SH matrix and floating away after gel dissolution; samples on i,iii) day 1 and ii,iv) day 7. Scales bars: A–E) 200 μm, I) 300 μm.

a separate mouse each, and a control of 200 000 suspended cells mixed 1:1 with Matrigel were subcutaneously injected into control mice. Matrigel is a basement membrane extract from mouse tumors, serving as a positive control for subcutaneous xenografts, and should show uniform tumor growth compared to the single face exposure from the PEG encapsulated microtumors.[36] Over the period of three weeks, tumor growth was measured daily with calipers. The control Matrigel samples were found to have the fastest growth profiles, followed by the hemisphere and the cubic aggregates respectively (Figure 4B). This can be related back to the Matrigel control, hemisphere and cubic tumors having decreasing surface area exposure of the cells respectively. As more of the tumor is confined within the nondegradable hydrogel construct, there will be less outgrowth compared to the cell suspension in Matrigel.

Technical replicates show slight variability in the growth rates of the tumor volumes which can be attributed to variations in tumors size changing the expected exposed surface area of 1.76 mm^2 for the hemisphere and 1.0 mm^2 for the cube (Figure S5, Supporting Information). To further quantitate

tumor growth, we performed ultrasound imaging and histopathology of excised tumor tissue. During tumor development, ultrasound images found differences in tumor vascularization among mice (Figure 4C). Ultrasound results show vascularization of both the initial seed tumor from within the matrix, but also the surrounding tissue outgrowth. When the percentage vascularity (PV) was analyzed for the entire tumor, variations can be seen between the hemisphere and cubic tumors measured with 6.881% and 1.707% vascularity respectively, which corresponds with the exposed tumor surface area. At the endpoint of the study, the mice where humanely sacrificed, and the tumor tissue paraffin fixed and embedded for histological analysis. Figure 4C shows the resected tumors, where the PEG gel remains visible at the base of tumor outgrowth. Consistent with the caliper measurements, both geometrically templated microtumors are considerably smaller than tumors from direct injection of tumor cells with Matrigel. Histology of microtumor samples demonstrate malignant melanoma invasion of the surrounding tissue with evidence for neovascularization (Figure 4D).
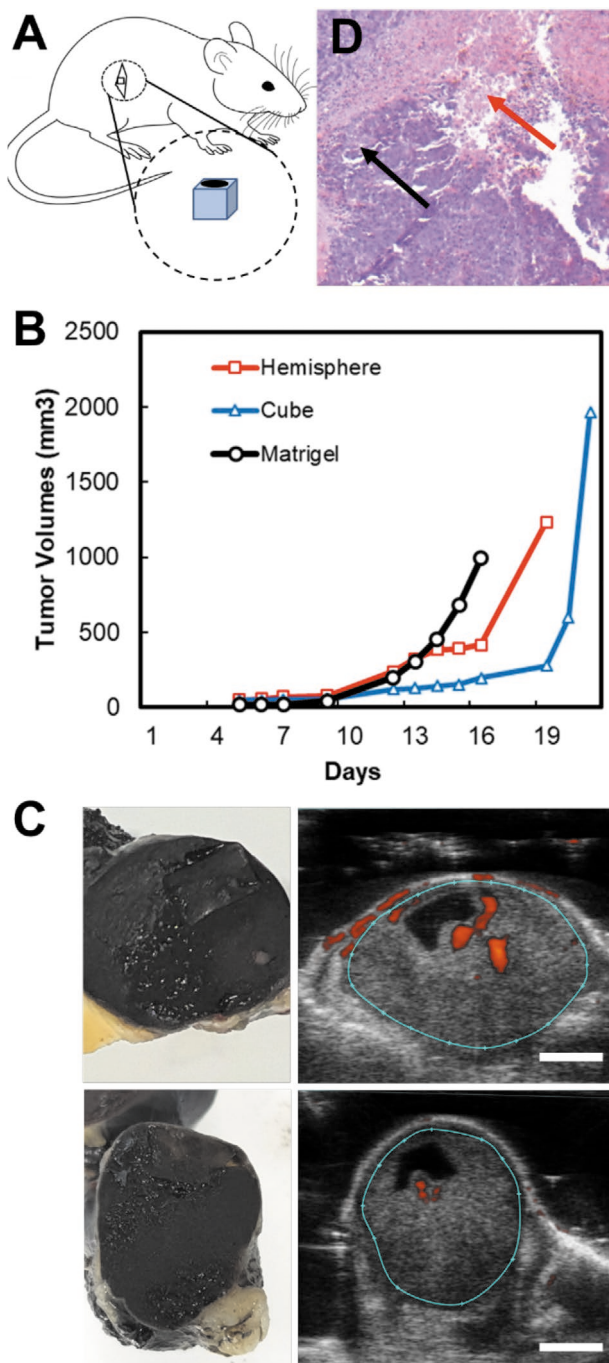
**ADVANCED
SCIENCE NEWS**

www.advancedsciencenews.com

**ADVANCED
BIOSYSTEMS**

www.adv-biosys.com

Figure 4. Subcutaneous implantation of microtumors in C57BL/6 mice. A) Schematic representing the implanted microtumor. B) Bulk tumor growth charts for a Matrigel control along with geometric structured microtumors. C) Optical images of cubic and hemisphere microtumors after excision from sacrificed mice along with ultrasound images show vascularity of the surrounding tumor. D) H & E staining of the outgrowth of a representative hemisphere tumor sample. The red arrow highlights regions of neovascularization around the tumor region. The black arrow corresponds to a region of tumor melanoma cells invading into the surround host tissue. Scale bars: C) 4.0 mm.

We have demonstrated a versatile approach for designing 3D printed structures that template virtually any biocompatible hydrogel material to create cell-laden microniches. Our approach is a simple, fast, and inexpensive method for creating geometrically defined tumor cell aggregates, enabling fundamental studies of the interplay between biophysical and biochemical cues during tumorigenesis in vitro and in vivo. This new platform enables the investigation into the roles that tumor volume, surface area, and geometry play in cancer progression. It additionally provides a pathway to precondition tumors prior to in vivo studies through control of matrix biophysical and biochemical parameters, hypoxic conditions, with potential for inclusion of other cell types. Growing microtumors in vitro within hydrogel templates allows translating a defined tumor architecture without disturbing cell-matrix and cell-cell interactions. Controlling the mechanics and chemistry of the template hydrogel, along with co-culture with multiple cell types, will facilitate fabrication of model tumor tissues with spatiotemporal control of heterogeneity. Templating more complex geometries allows for culturing tumor cells in a native topology compared to commonly used spheroids, i.e., multiarmed structure of glioblastoma, spatial distribution of stroma in pancreatic cancer, etc. Finally, advances in multimodal imaging and 3D printing techniques holds the potential for translating in vivo clinical images of patient tumors to printable templates, enabling replication of clinically relevant architectures for crafting individualized drug development models.

Experimental Section

Synthesis of Templates and Templated Hydrogels: The template designs were created in Inventor CAD software 2018. Exported design files were sent to the rapid prototyping lab at the University of Illinois Urbana-Champaign where they were printed using a Viper Si Stereolithographic 3D printer. For fabrication of the hydrogel wells, the templates were then pressed into a watertight mold. A 10 wt% solution of poly(ethylene glycol) dimethacryloyl (PEGDM) (10 kDa) was dissolved in deionized (DI) water followed by degassing with ultra-high purity Argon for 10 min. For crosslinking, a 10% solution ammonium persulfate (Chem-Supply Pty Ltd Australia, 473645) and pure N,N,N',N'-tetramethylethylenediamine (TEMED) (Sigma Aldritch, 636320) were added to the PEGDM hydrogel solution in a 5:1:250 ratio respectively and immediately added over the template to gel. After 30 min, the templates were popped out of the models and the hydrogels were gently peeled off. The gels were then placed on a shaker for 45 min with a 25 µg mL^{-1} solution of bovine fibronectin in each of the wells. Gels were subsequently stored submerged in DI water at 4 °C until further use. For the disulfide gels, a 15 wt% solution of four-arm PEG-SH (5 kDa JenKem Technology) was dissolved in DI water. For crosslinking, a 1 M sodium iodide solution (Sigma Aldritch, 383112) and a 30 wt% solution of hydrogen peroxide (Sigma Aldritch, H1009) were added to the prehydrogel solution in a 1:10:1000 ratio, respectively. The gels were added over the molds and allowed to crosslink for 2 h before removal. Protocols for PEGDM and GelMa synthesis were adapted from previous reports[37–39] and details can be found in Supporting Information.

Cell Culture and Seeding: The cancer cell line B16F0 (murine melanoma) was purchased from American Type Culture Collection (ATCC). Cells were cultured at 37 °C with 5% CO_2 and 100% humidity in Dulbecco's modified Eagle medium (DMEM) (10% FBS and 1% penicillin/streptomycin) and were passaged at ≈80% confluency. Media was changed every 2–3 d and cell passages 5–17 were used for this study. The cells were mycoplasma tested with MycoAlert Mycoplasma Detection Kit (Lonza, LT07-318) prior to in vitro or in vivo studies.

For seeding the microtumors, DMEM media with 1% P/S and 20% FBS was used. Cultured cells were trypsinized and pelleted down in a centrifuge tube where the supernatant was removed. The cell pellet was subsequently pipetted directly into the templated hydrogel wells. 2 mL of media were slowly added to the wells to prevent disturbing the tumors. Tumors were cultured for 5 d with media changes on days 1 and 3.

Lightsheet Imaging: For all lightsheet images, the Zeiss Z.1 lightsheet was used. Cleared tumor samples were mounted onto custom 3D printed mounts (Figure S6, Supporting Information). Samples were then loaded into the instrument in a chamber filled with the cubic clearing solution 2 to match indices of refraction. For 5× images and 20× objectives, 5× and 10× lightsheet focusing objectives were used, respectively. Lightsheet thicknesses of 2.5 and 4 µm were used along with pivot scan. Images were only taken from the left side unless specified otherwise. Nyquist resolution was used to determine z-slice thicknesses.

B16 Murine Melanoma In Vivo Models: Eight 6 week C57BL/6 mice were obtained from the Animal Resources Centre (Perth, Australia). After 7 d acclimatization, mice were randomly divided into four groups (n = 2): star, hemisphere, cube, and nonpattern control (Matrigel). Different shaped hydrogel or Matrigel with murine melanoma cells B16F0 were implanted subcutaneously into the right flank of the mouse. Mice were monitored daily for any loss of condition, and tumor progression was documented by measurements using electronic calipers in two dimensions (d1 and d2) and the volume (V) was calculated by the standard formula for an ellipse: $V = 1/6\ \pi (d1 \times d2)^{3/2}$. Ultrasound was also used to monitor the tumor for size changes and vascularity measurement with Power Doppler. Individual mice were euthanized once their tumor reached about 1000 mm^3, according to ethics considerations. At the end point, tumors were measured, weighted, and harvested for the further histology analysis.

Ethics Statement: All animal experiments were approved (ACEC #18/105B) by UNSW Animal Care and Ethics Committee.

Supporting Information

Supporting Information is available from the Wiley Online Library or from the author.

Acknowledgements

Conflict of Interest

The authors declare no conflict of interest.

Keywords

[1] M. W. Tibbitt, K. S. Anseth, *Biotechnol. Bioeng.* **2009**, *103*, 655.
[2] S. Breslin, L. O'Driscoll, *Drug Discovery Today* **2013**, *18*, 240.
[3] A. D. Doyle, N. Carvajal, A. Jin, K. Matsumoto, K. M. Yamada, *Nat. Commun.* **2015**, *6*, 8720.
[4] G. Hamilton, *Cancer Lett.* **1998**, *131*, 29.
[5] S. Nath, G. R. Devi, *Pharmacol. Ther.* **2016**, *163*, 94.
[6] G. Mehta, A. Y. Hsiao, M. Ingram, G. D. Luker, S. Takayama, *J. Controlled Release* **2012**, *164*, 192.
[7] J. Lee, A. A. Abdeen, J. Hedhli, K. L. Wycislo, I. T. Dobrucka, T. M. Fan, L. W. Dobrucki, K. A. Kilian, *Sci. Adv.* **2017**, *3*, e1701350.
[8] J. Lee, A. A. Abdeen, K. L. Wycislo, T. M. Fan, K. A. Kilian, *Nat. Mater.* **2016**, *15*, 856.
[9] M. Bao, J. Xie, A. Piruska, W. T. S. Huck, *Nat. Commun.* **2017**, *8*, 1962.
[10] A. P. Zhang, X. Qu, P. Soman, K. C. Hribar, J. W. Lee, S. Chen, S. He, *Adv. Mater.* **2012**, *24*, 4266.
[11] R. Gauvin, Y.-C. Chen, J. W. Lee, P. Soman, P. Zorlutuna, J. W. Nichol, H. Bae, S. Chen, A. Khademhosseini, *Biomaterials* **2012**, *33*, 3824.
[12] S. J. Bryant, J. L. Cuy, K. D. Hauch, B. D. Ratner, *Biomaterials* **2007**, *28*, 2978.
[13] K. C. Hribar, P. Soman, J. Warner, P. Chung, S. Chen, *Lab Chip* **2014**, *14*, 268.
[14] G. Wu, Y. Xia, S. Yang, *Soft Matter* **2014**, 1392.
[15] B. C. Gross, J. L. Erkal, S. Y. Lockwood, C. Chen, D. M. Spence, *Anal. Chem.* **2014**, *86*, 3240.
[16] A. Revzin, R. J. Russell, V. K. Yadavalli, W.-G. Koh, C. Deister, D. D. Hile, M. B. Mellott, M. V. Pishko, *Langmuir* **2001**, *17*, 5440.
[17] M. S. Hahn, L. J. Taite, J. J. Moon, M. C. Rowland, K. A. Ruffino, J. L. West, *Biomaterials* **2006**, *27*, 2519.
[18] G. M. Cruise, D. S. Scharp, J. A. Hubbell, *Biomaterials* **1998**, *19*, 1287.
[19] A. V. Salvekar, W. M. Huang, R. Xiao, Y. S. Wong, S. S. Venkatraman, K. H. Tay, Z. X. Shen, *Acc. Chem. Res.* **2017**, *50*, 141.
[20] A. A. Yazdi, A. Popma, W. Wong, T. Nguyen, Y. Pan, J. Xu, *Microfluid. Nanofluid.* **2016**, *20*, 50.
[21] L. le Roux, A. Volgin, D. Maxwell, K. Ishihara, J. Gelovani, D. Schellingerhout, *Mol. Imaging* **2008**, *7*, 7290.2008.00023.
[22] D. S. Richardson, J. W. Lichtman, *Cell* **2015**, *162*, 246.
[23] K. Chung, J. Wallace, S.-Y. Kim, S. Kalyanasundaram, A. S. Andalman, T. J. Davidson, J. J. Mirzabekov, K. A. Zalocusky, J. Mattis, A. K. Denisin, S. Pak, H. Bernstein, C. Ramakrishnan, L. Grosenick, V. Gradinaru, K. Deisseroth, *Nature* **2013**, *497*, 332.
[24] B. Yang, J. B. Treweek, R. P. Kulkarni, B. E. Deverman, C.-K. Chen, E. Lubeck, S. Shah, L. Cai, V. Gradinaru, *Cell* **2014**, *158*, 945.
[25] T. Kuwajima, A. A. Sitko, P. Bhansali, C. Jurgens, W. Guido, C. Mason, *Development* **2013**, *140*, 1364.
[26] E. A. Susaki, K. Tainaka, D. Perrin, F. Kishino, T. Tawara, T. M. Watanabe, C. Yokoyama, H. Onoe, M. Eguchi, S. Yamaguchi, T. Abe, H. Kiyonari, Y. Shimizu, A. Miyawaki, H. Yokota, H. R. Ueda, *Cell* **2014**, *157*, 726.
[27] E. A. Susaki, K. Tainaka, D. Perrin, H. Yukinaga, A. Kuno, H. R. Ueda, *Nat. Protoc.* **2015**, *10*, 1709.
[28] C.-H. Liu, C.-H. Lin, M.-J. Tsai, Y.-H. Chen, S.-F. Yang, K.-B. Tsai, *Int. J. Surg. Pathol.* **2018**, *26*, 410.
[29] M. Grimm, M. Krimmel, J. Polligkeit, D. Alexander, A. Munz, S. Kluba, C. Keutel, J. Hoffmann, S. Reinert, S. Hoefert, *Eur. J. Cancer* **2012**, *48*, 3186.
[30] K. Yue, G. T.-D. Santiago, M. M. Alvarez, A. Tamayol, N. Annabi, A. Khademhosseini, *Biomaterials* **2015**, *73*, 254.
[31] K. S. Kopanska, Y. Alcheikh, R. Staneva, D. Vignjevic, T. Betz, *PLoS One* **2016**, *11*, e0156442.

[32] R. S. H. Chang, J. C.-W. Lee, S. Pedron, B. A. C. Harley, S. A. Rogers, *Biomacromolecules* **2019**, *20*, 2198.

[33] M. Kar, Y.-R. V. Shih, D.O Velez, P. Cabrales, S. Varghese, *Biomaterials* **2016**, *77*, 186.

[34] M. M. Jensen, J. T. Jørgensen, T. Binderup, A. Kjær, *BMC Med. Imaging* **2008**, *8*, 16.

[35] K. Mekada, K. Abe, A. Murakami, S. Nakamura, H. Nakata, K. Moriwaki, Y. Obata, A. Yoshiki, *Exp. Anim.* **2009**, *58*, 141.

[36] H. K. Kleinman, G. R. Martin, *Semin. Cancer Biol.* **2005**, *15*, 378.

[37] S. Lin-Gibson, S. Bencherif, J. A. Cooper, S. J. Wetzel, J. M. Antonucci, B. M. Vogel, N. R. Washburn, *Biomacromolecules* **2004**, *5*, 1280.

[38] J. W. Nichol, S. T. Koshy, H. Bae, C. M. Hwang, S. Yamanlar, A. Khademhosseini, *Biomaterials* **2010**, *31*, 5536.

[39] H. Shirahama, B. H. Lee, L. P. Tan, N.-J. Cho, *Sci. Rep.* **2016**, *6*, 31036.